Journal of New Technology and Materials
JNTM
Vol. 04, N°01 (2014)23-26

OEB Univ. Publish. Co.

Design and simulation of a valveless piezoelectric micropump for fuel delivery in fuel cell devices

Yasser Rihan
Associate Prof., Atomic Energy Authority, Egypt.

Received: 30 April 2014, accepted 26 May 2014

Abstract

Micro- and nano-electromechanical systems (MEMS or NEMS)-based fuel delivery in direct methanol fuel cell (DMFC) devices offer opportunities to address unmet fuel cells related to fuel delivery. By applying an alternating electrical field across the actuator, the resultant reciprocating movement of the pump diaphragm can be converted into pumping effect. Nozzle/diffuser elements are used to direct the flow. To make the power system applicable for portable electronic devices, the micropump needs to meet some specific requirements: low power consumption but sufficient fuel flow rate. In this study, a theoretical method have been used to investigate the effects of materials properties, actuator dimensions, driving voltage, driving frequency, nozzle/diffuser dimension, and other factors on the performance of the whole system. As a result, a viable design of micropump system for fuel delivery in DMFC devices has been achieved and some further improvements are suggested. A mathematical model was used to simulate the behaviour of the micropump. The results of mechanical calculations and simulations show good agreement with the actual behaviour of the pumps.

Keywords: Simulation; micropump; piezoelectric; fuel cell.

1. Introduction

The piezoelectric effect is the ability of certain materials to produce an electric charge proportional to an applied mechanical stress. This is known as the direct piezoelectric effect. The electric charge can also be produced in the reverse direction, by reversing the direction of applied stress. The piezoelectric effect is reversible which implies that when an electric field is applied a mechanical strain is created in the material. The piezoelectric effect is defined as a linear relationship between a mechanical variable and an electric variable. Piezoelectric thick films are of major interest in the actuation of active structures in MEMS, they have been widely applied to micropumps, ultrasonic motors, resonators, microfluidic separators, high-frequency transducers, and energy harvesting, [1] because they exhibit properties such as larger displacement and quick response, high frequency, and can be precisely controlled.

The development of pumping devices in microscale is a part of the emerging research field of microfluidics [2]. Besides stand-alone micropumps, simple pump designs are required for integration in miniaturized chemical analyzers, which are often called micro total analysis systems (μTAS) or lab on a chip (LOC). Low-voltage and low-power actuating schemes for the pump are needed for the use in hand-held devices which are usually powered by batteries.

Micropumps with surface mounted piezoelectric membrane actuation were first reported by van Lintel et al. [3]. Piezopumps have been considerably developed over the past several years. They have many excellent abilities such as liquid handling in small and precise volume, providing a high actuation force with a relative fast mechanical response at high operation frequency, and miniaturization in a small size, etc. [4–6]. Therefore, they are able to serve in chemical, medical, and biomedical applications with great scientific and commercial potential [7–9].

A fuel cell is a kind of electrochemical device that converts the chemical energy of reactants directly into electricity, which offers advantages of high energy density, low volume and weight, no moving parts and no harmful emissions. Recently, miniature fuel cells have been drawing increasing attention as a possible solution to the search for improved power sources for portable power systems [10]. The direct methanol fuel cell (DMFC) is one of the fuel cells which have the potential to be miniaturized. The chemical reaction in DMFC is as follows:

Anode: $CH_3OH + H_2O \rightarrow CO_2 + 6H^+ + 6e^-$

Cathode: $3/2O_2 + 6H^+ + 6e^- \rightarrow 3H_2O$

Overall reaction: $CH_3OH + 3/2O_2 \rightarrow CO_2 + 2H_2O$

From the equation above, it holds true that in a completely passive system, the entire surface area of the fuel cell cathode must be exposed to the exterior to allow air to reach the catalyst layer. For longer durations, however, in the absence of convection, the local oxygen concentration adjacent to the cathode will be depleted. So, one of the key technologies has been that of an active air

supply device which can feed sufficient air into the DMFC pack.

The cross-section of the DMFC power system with valveless piezoelectric micropump is shown schematically in Fig. 1. This system mainly consists of the following parts: fuel cell membrane electrode assembly (MEA), fuel chamber, nozzle/diffuser, micropump and pump chamber, and fuel supply manifold. All these parts are fabricated in a multi-layer structure to obtain a compact system. The fuel cell MEA is made of a Nafion117 membrane layer sandwiched by two electrode layers with catalysts deposited on them. And the micropump is fabricated by bonding a thin piezoelectric disk on a metal diaphragm. When applying an alternating voltage to the piezoelectric disk, the diaphragm is actuated to produce bending deformation that causes the volume change of pump chamber. By selecting appropriate shape and dimension of the nozzle/diffuser between pump chamber and fuel chamber, the fuel can circulate in the desired direction. And the fuel supply from the right chamber can compensate the fuel consumption.

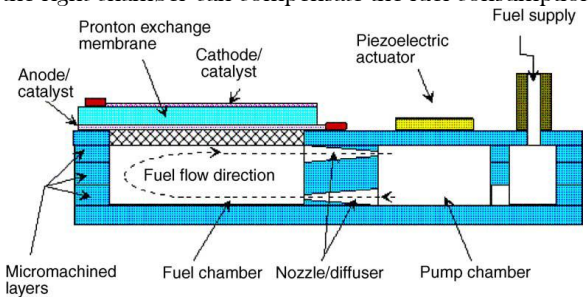

Fig. 1: Schematic of the miniaturized DMFC system driven by piezoelectric valveless micropump.

2. Model of micropump

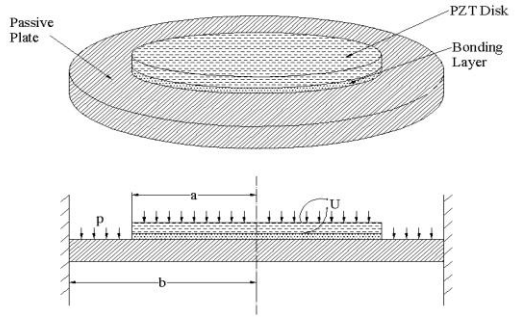

Fig. 2: Schematic of the piezoelectric micropump actuator.

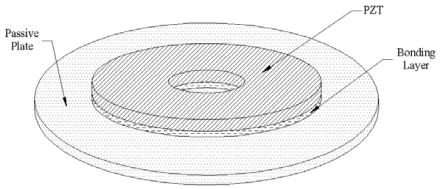

Fig. 2(a): Disk-type bending actuator.

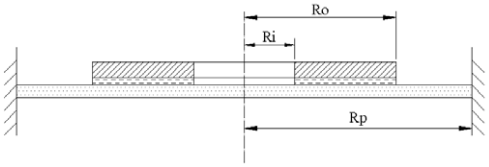

Fig. 2(b): Ring-type bending actuator.

The most important part of a micropump is the actuator, which in this case is actually a piezoelectric bending actuator made of three layers: PZT layer, bonding layer and passive plate. When applying an alternating electrical field across the PZT layer, it will generate a reciprocating deflection in the direction vertical to the surface of the actuator. This deflection is then transferred to the pumping effect that drives the fluid inside the pump chamber flowing through the inlet/outlet. Therefore the first thing need to do in the micropump modeling is to calculate this deflection. In most of the applications for micropumps, the PZT disk is smaller than the passive plate and therefore the edge of the PZT disk is often considered to be free. The schematic of the actuator part is illustrated in Fig. 2. As shown in the figure, the PZT disk is adhered to the passive plate by a thin layer of conductive epoxy.

The modeling process can be simplified assuming the whole structure is circumferentially symmetrical, the bonding between the PZT disk and the passive plate is perfect and the outer edge of the passive plate is fixed.

2.1. Desk-type deflection

The model developed by [11] for deflection caused by the applied voltage can be adopted here directly. The intermediate moment caused by the actuation of the PZT is:

$$M_0 = D_e \frac{-d_{31}U/h_{pzt}}{\frac{h}{2}+\frac{2}{h}\left(\frac{1}{E_{pzt}h_{pzt}}+\frac{1}{E_p h_p}\right)\left(D_{pzt}+D_p\right)} \quad (1)$$

The bonding moment M_1, as delivered by Li et al [12] is:

$$M_1 = \frac{\eta d_{31}U\left(2h'+2h_p+h_{pzt}\right)\left(h'^3+h^3\right)}{2\left[h^3+(1-\alpha)h'^3+(\alpha-\beta)\left(h'+h_p\right)^3+\beta\left(h'+h_p+h_{pzt}\right)^3\right]} \quad (2)$$

where,

$$\eta = \frac{E_{pzt}}{1-\gamma_{pzt}^2},\ h' = h_p - h,\ \alpha = \frac{1-\gamma_p^2}{1-\gamma_b^2}\frac{E_b}{E_p},\ \beta = \frac{1-\gamma_p^2}{1-\gamma_{pzt}^2}\frac{E_{pzt}}{E_p}$$

The defection can be determined by the following equations:

$$W_1(r) = \frac{M_{11}a^2}{2D_p\left[(1-\gamma_p)b^2+(1+\gamma_p)a^2\right]}\times\left(-r^2+2b^2\log\frac{r}{b}+b^2\right) \quad (3)$$

The deflection W_2 for the three-layer structure can be expressed as follows [13]:

$$W_2(r) = \frac{M_{11}b^2}{2D_p\left[(1-\gamma_p)b^2+(1+\gamma_p)a^2\right]}\times\left(-a^2+2b^2\log\frac{a}{b}+b^2\right) \quad (4)$$

$$+\frac{M_1}{2D_c(1+\gamma_c)}\left(a^2-r^2\right)$$

The continuity condition is:

$$\left.\frac{dW_1(r)}{dr}\right|_{r=a} = \left.\frac{dW_2(r)}{dr}\right|_{r=a} \quad (5)$$

The moment M_{11} can be expressed as follows:

$$M_{11} = -\frac{M_1 D_p\left[(1-\gamma_p)b^2+(1-\gamma_p)a^2\right]}{D_c(1+\gamma_c)\left(b^2-a^2\right)} \quad (6)$$

The deflection equation can be rewritten as:

$$W_1(r) = \frac{M_1 a^2\left(r^2-2b^2\log r/b-b^2\right)}{2D_c(1+\gamma_c)\left(b^2-a^2\right)},\ (a\le r\le b) \quad (7)$$

$$W_2(r) = \frac{M_1\left[\left(b^2-a^2\right)\left(a^2-r^2\right)+a^2\left(a^2-2b^2\log a/b-b^2\right)\right]}{2D_c(1+\gamma_c)\left(b^2-a^2\right)},$$

$$(0\le r\le a) \quad (8)$$

Under constant pressure difference p, the deflection of the passive plate is:

$$W_3(r)=\frac{p}{64D_p}\left(b^2-r^2\right)^2+\frac{(M_{21}-M_2)a^2\left(r^2-2b^2\log r/b-b^2\right)}{2D_p\left[(1-\gamma_p)b^2+(1+\gamma_p)a^2\right]} \quad (9)$$

Where M_2 and M_{21} are two intermediate bending moments, the continuity condition of the slope of the deflection at $r = a$ can be used to determine M_2 and the other moment can be expressed as:

$$M_{21}=\frac{p}{16}\left[(1+\gamma_p)b^2-(3+\gamma_p)a^2\right] \quad (10)$$

The deflection of the three-layer structure can be expressed as follows:

$$W_4(r)=\frac{p}{64D_p}\left(b^2-a^2\right)^2+\frac{(M_{21}-M_2)a^2\left(a^2-2b^2\log a/b-b^2\right)}{2D_p\left[(1-\gamma_p)b^2+(1+\gamma_p)a^2\right]}+\frac{p\left(a^2-r^2\right)}{64D_p}\left(\frac{5+\gamma_c}{1+\gamma_c}a^2-r^2\right)+\frac{M_2\left(a^2-r^2\right)}{2D_c(1+\gamma_c)}. \quad (11)$$

For the bonding material, the stress follows:

$$\sigma_b=\frac{E_b}{1-\gamma_b}\varepsilon_b \quad (12)$$

where ε_b is the strain of the bonding material.

2.2. Ring-type deflection

Assuming the whole system is linear, the deflection equations for the ring-type actuator can be expressed as follow:

$$W_1(r)=\frac{M_0\left[(R_p^2-R_0^2)(R_0^2-r^2)+R_0^2\left(R_0^2-2R_p^2\log(R_0/R_p)-R_p^2\right)\right]}{2\left\{D_p\left[(1+\gamma_p)R_0^2+(1-\gamma_p)R_p^2\right]+D_e(1+\gamma_e)(R_p^2-R_0^2)\right\}}-\frac{M_0\left[(R_p^2-R_i^2)(R_i^2-r^2)+R_i^2\left(R_i^2-2R_p^2\log(R_i/R_p)-R_p^2\right)\right]}{2\left\{D_p\left[(1+\gamma_p)R_i^2+(1-\gamma_p)R_p^2\right]+D_e(1+\gamma_e)(R_p^2-R_i^2)\right\}},\quad (0\le r\le R_i) \quad (13)$$

$$W_2(r)=\frac{M_0\left[(R_p^2-R_0^2)(R_0^2-r^2)+R_0^2\left(R_0^2-2R_p^2\log(R_0/R_p)-R_p^2\right)\right]}{2\left\{D_p\left[(1+\gamma_p)R_0^2+(1-\gamma_p)R_p^2\right]+D_e(1+\gamma_e)(R_p^2-R_0^2)\right\}}-\frac{M_0R_i^2\left(r^2-2R_p^2\log(r/R_p)-R_p^2\right)}{2\left\{D_p\left[(1+\gamma_p)R_i^2+(1-\gamma_p)R_p^2\right]+D_e(1+\gamma_e)(R_p^2-R_i^2)\right\}},\quad (R_i\le r\le R_0) \quad (14)$$

$$W_3(r)=\frac{M_0R_0^2\left(r^2-2R_p^2\log(r/R_p)-R_p^2\right)}{2\left\{D_p\left[(1+\gamma_p)R_0^2+(1-\gamma_p)R_p^2\right]+D_e(1+\gamma_e)(R_p^2-R_0^2)\right\}}-\frac{M_0R_i^2\left(r^2-2R_p^2\log(r/R_p)-R_p^2\right)}{2\left\{D_p\left[(1+\gamma_p)R_i^2+(1-\gamma_p)R_p^2\right]+D_e(1+\gamma_e)(R_p^2-R_i^2)\right\}},\quad (R_0\le r\le R_p) \quad (15)$$

The deflection caused by pressure difference can be expressed similar to the case of disk-type actuator; the deflection induced by mechanical pressure can be determined by using the superposition method as follows:

$$W_4(r)=W_5(R_i)+\frac{p\left(R_i^2-r^2\right)}{64D_p}\left(\frac{5+\gamma_p}{1+\gamma_p}R_i^2-r^2\right)+\frac{M_1\left(R_i^2-r^2\right)}{2D_p(1+\gamma_p)},\quad (0\le r\le R_i) \quad (16)$$

$$W_5(r)=W_6(R_0)+\frac{p\left(R_0^2-r^2\right)}{64D_e}\left(\frac{5+\gamma_e}{1+\gamma_e}R_0^2-r^2\right)+\frac{\left(R_0^2M_2-R_i^2(M_1-M')\right)\left(R_0^2-r^2\right)}{2D_e(1+\gamma_e)\left(R_0^2-R_i^2\right)}-\frac{R_0^2R_i^2(M_2-M_1+M')\log(r/R_0)}{D_e(1-\gamma_e)\left(R_0^2-R_i^2\right)},\quad (R_i\le r\le R_0) \quad (17)$$

$$W_6(r)=\frac{p\left(R_p^2-r^2\right)^2}{64D_p}+\frac{(M''-M_2)R_0^2\left(r^2-2R_p^2\log(r/R_p)-R_p^2\right)}{2D_p\left[(1-\gamma_p)R_p^2+(1+\gamma_p)R_0^2\right]},\quad (R_0\le r\le R_p) \quad (18)$$

Where, M' and M'' are two intermediate bending moments, of which

$$M'=p(3+\gamma_e)\left(R_0^2-R_i^2\right)/16 \quad (19)$$

$$M''=p\left[R_p^2(1+\gamma_p)-R_0^2(3+\gamma_p)\right]/16 \quad (20)$$

The relation between the total generated current and the methanol solution flow rate can be written as:

$$I=Q\times D_M\times 6\times F \quad (21)$$

(where D_M is the mole density of methanol solution and F is Faraday's constant).

3. Model validation and predicted results

Water is used as working fluid whose property is quite close to that of the methanol water solution. Comparison between the measured water flow-rate [14] under different pressure head were compared with the predicted results as shown in Figure 3. The larger flow rate corresponds to the lower pressure head. As shown in the figure there is a good agreement between the experimental and predicted results.

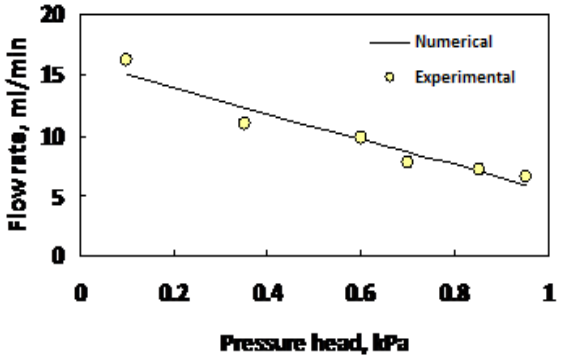

Fig. 3: Flow rate versus pressure head, f = 200 Hz.

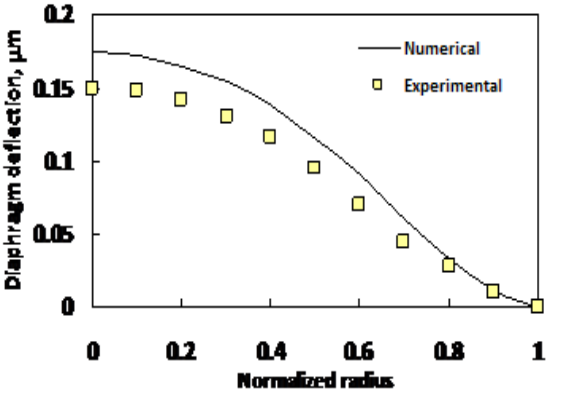

Fig. 4: Comparison between experimental and numerical results of the diaphragm deflections.

Figure 4 shows a comparison of the deflection of the diaphragm between the predicted results of the present model and the experimental results of Zhang et al. [15]. The predicted results have the same trend of the experimental data and the maximum deflection always appears at the center. The numerical deflection is smaller than the experimental this may tends to the fabrication process may result in some residual stress or strain and the boundary conditions are not ideal fixed. Also the actual deformation of the bending actuator in three-dimensional but the numerical result is two-dimensional. Furthermore, there may be defections and non-uniformities in the materials used for experiments therefore the experimental data will not be accurate.

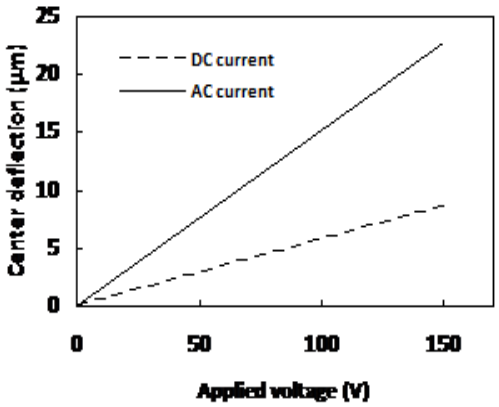

Fig. 5: Center deflection results of the diaphragm under different voltage.

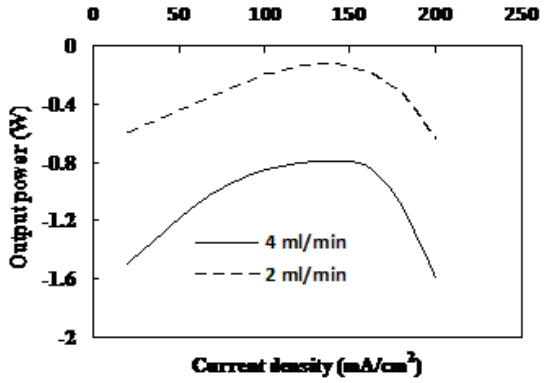

Fig. 6: Output power under different operation conditions, f= 100 Hz.

The predicted center deflection of the micropump and the applied voltage is linear as shown if Fig. 5. Increasing the applied voltage will increase the applied electric field; therefore the deflection and the volume displacement will increase. The applied electrical field cannot exceed a certain limit or the PZT material will be depolarized. The applied AC voltage is sinusoidal and the frequency is 100 Hz give much larger deflections as shown in Fig. 5. The output power under different conditions consumed by the piezoelectric micropump from the total power generated by fuel cell is shown in Fig.6. The power generated by the fuel cell is not enough to drive the micropump for both 2 and 4 ml/min then the flow rate must be less than these values to get positive output power.

4. Conclusions

This research is focused on the development of a valveless piezoelectric micropump for miniaturized direct methanol fuel cell system as power source for portable electronics. A theoretical study is conducted to design, optimize, and characterize such a system. This work demonstrates that the working principle of the whole system design is sound and viable. A mathematical model was used to simulate the behavior of the micropump. The results of mechanical calculations and simulations show good agreement with the actual behavior of the pumps.

References

[1] T. Yan, B.E. Jones, R.T. Rakowski, M.J. Tudor, S.P. Beeby, N.M. White, Sens. Actuators A, 115 (2004) 401.
[2] N.T. Nguyen, S.T. Wereley, Fundamentals and Applications of Microfluidics, 1st ed., Artech House, Boston, MA, 2002.
[3] H.T.G. van Lintel, F.C.M. vande Pal, S. Bouwstra, Sensors and Actuators, 15 (2) (1988) 153.
[4] P. Woias, Sens. Actuators B: Chem., 105 (1) (2005) 28.
[5] D.J. Laser, J.G. Santiago, J. Micromech. Microeng., 14 (6) (2004) 35.
[6] N.T. Nguyen, X.Y. Huang, T.K. Chuan, J. Fluids Eng. Trans., ASME, 124 (2) (2002) 384.
[7] D.A. Henderson, NSTI Nanotechnol. Conf. Trade Show Technol. Proc., 3 (2007) 272.
[8] S.B. Choi, J.K. Yoo, M.S. Cho, Y.S. Lee, Mechatronics, 15 (2) (2005) 239.
[9] E.G. Chapman, S.L. Herdic, C.A. Keller, C.S. Lynch, Proc. SPIE Int. Soc. Opt. Eng., 5762 (2005) 299.
[10] K. Cowey, K.J. Green, G.O. Mepsted, R. Reeve, Curr. Opin. Solid State Mater. Sci., 8 (2004) 367.
[11] B. Minqiang, T. Melvin, G. Ensell, J. Wilkinson, A.G. Evans, Journal of Micromechanics and Microengineering, 13 (2003) S125.
[12] S. Li, S. Chen, Sens. Actuators A, 104 (2003) 151.
[13] S. Timoshenko, S. Woinowsky-Krieger, Theory of plates and shells, Second ed., McGraw-Hill, New York, 1959.
[14] M. Richter, R. Linnemann, P. Woias, Sensors and Actuators A, 68 (1998) 480.
[15] T. Zhang, Q. Wang, , J. of Power Sources, 140 (2005) 72.